Universiteit Antwerpen

This item is the archived preprint of:

Exit wave reconstruction from focal series of HRTEM images, single crystal XRD and total energy studies on Sb_xWO_{3+y} ($x \sim 0.11$)

Reference:

Klingstedt Miia, Sundberg Margareta, Eriksson Lars, Haigh Sarah, Kirkland Angus, Grüner Daniel, de Backer Annick, Van Aert Sandra, Tarasaki Osamu.- Exit wave reconstruction from focal series of HRTEM images, single crystal XRD and total energy studies on Sb_xWO_{3+y} ($x \sim 0.11$)

Zeitschrift für Kristallographie - ISSN 0044-2968 - 227:6(2012), p. 341-349

Full text (Publishers DOI): http://dx.doi.org/doi:10.1524/zkri.2012.1517

To cite this reference: http://hdl.handle.net/10067/1012180151162165141

uantwerpen.be

Institutional repository IRUA

Exit wave reconstruction from focal series of HRTEM images, single crystal XRD and total energy studies on Sb_xWO_{3+y} (x~0.11)

Miia Klingstedt[I], Margareta Sundberg[I,*], Lars Eriksson[I], Sarah Haigh[II,III], Angus Kirkland[II], Daniel Grüner[IV], Annick De Backer[V], Sandra Van Aert[V] and Osamu Terasaki[I,VI,*]

[I] Department of Materials and Enviromental Chemistry, Stockholm University, SE-106 91, Stockholm, Sweden.

[II] Department of Materials, University of Oxford, Parks Road, Oxford, OX1 3PH U.K.

[III] Now at The University of Manchester , Materials Science Centre, Grosvenor Street, Manchester, M1 7HS, U.K.

[IV] Max Planck Institute for Chemical Physics of Solids, Nöthnitzer Str. 40, D-01187 Dresden, Germany.

[V] Electron Microscopy for Materials Research (EMAT), University of Antwerp, Groenenborgerlaan 171, 2020 Antwerp, Belgium

[VI] Graduate School of EEWS, WCU Energy Science and Engineering, N5-Building 335 Gwahangno, Yuseong-Gu 305-701, Daejeon, Rebublic of Korea.

*Corresponding authors: margareta.sundberg@mmk.su.se, terasaki@mmk.su.se
Received; accepted

Abstract.
A new tungsten bronze in the Sb-W-O system has been prepared in a solid state reaction from Sb_2O_3, WO_3 and W metal powder. The average structure was determined by single crystal X-ray diffraction. Sb_xWO_{3+y} (x~0.11) crystallizes in the orthorhombic space group $Pm2_1n$ (no. 31), a = 27.8135(9) Å, b = 7.3659(2) Å and c = 3.8672(1) Å. The structure belongs to the (*n*)-ITB class of intergrowth tungsten bronzes. It contains slabs of hexagonal channels formed by six WO_6 octahedra. These slabs are separated by three layers of WO_6 octahedra that are arranged in a WO_3-type fashion. The WO_6 octahedra share all vertices to build up a three-dimensional framework. The hexagonal channels are filled with Sb atoms to ~80% and additional O atoms. The atoms are shifted out of the center of the channels. Exit-wave reconstruction of focal series of high resolution-transmission–electron- microscope (HRTEM) images combined with statistical parameter estimation techniques allowed to study local ordering in the channels. Sb atoms in neighbouring channels tend to be displaced in the same direction, which is in agreement with total energy calculations on ordered structure models, but the ratio of the occupation of the two possible Sb sites varies from channel to channel. The structure of Sb_xWO_{3+y} exhibits pronounced local modulations.

Introduction

The tungsten bronzes form a group of structurally complex and non-stoichiometric oxides with the general formula M_xWO_3, $0 < x < 1$ where M typically is an electropositive metal (in this study M = Sb) [1]. Sodium tungsten bronzes were prepared by Wöhler as early as 1823. They were given the name bronze due to their characteristic metallic shimmer and intense colour. The tungsten bronzes are chemically inert and electrically conductive. They have recently attracted significant interest as a result of their application as the oxygen electrode in fuel cells utilizing an acid electrolyte [2,3]. Other applications of these materials include electrochromic devices [4] and humidity sensors [5]. Mixed oxide catalysts containing Sb and W are composed of a variety of phases, including tungsten bronzes [6].

Tungsten bronzes adopt four different structure types. These are, perovskite tungsten bronzes (PTB), tetragonal tungsten bronzes (TTB), hexagonal tungsten bronzes (HTB) [7] and intergrowth tungsten bronzes (ITB) [8]. All four structure types are built up of corner-sharing WO_6-octahedra arranged in a three dimensional network, that gives rise to various kinds of tunnels or cages where the electropositive M atoms can be located. The ITB phases are constructed of 2-dimensionally infinite slabs of distorted WO_3-type intergrown with HTB-type slabs. The width of both type of slabs can vary, which will give rise to both ordered and disordered

structures. In the (*n*)-ITB structure the HTB-type slabs are one hexagonal tunnel row wide and the width of the WO_3-type slab is equal to *n* octahedra. The WO_3-type slabs in the (2)-ITB structure are thus two octahedra wide. This structure has previously been reported for $Sb_{0.16}WO_3$ [9] Tungsten bronze structures containing antimony are interesting from a structural point of view for the following reasons. First, Sb atoms in the common oxidation state +III carry a lone pair of electrons, which can be stereochemically active [9]. Second, oxygen atoms can be incorporated together with Sb into the channels of the HTB slabs, forming angulate Sb_2O units as observed for the (2)-ITB phase in the system Sb-Mo-O [10]. Third, Sb atoms are likely to form covalent bonds with the O atoms of the tungsten bronze framework. All these features result in a rather strong interaction between the tungsten bronze host and the Sb guest atoms inside the channels. Therefore, one can expect pronounced local structural modulations, especially local variation in the antimony occupancy and oxygen sites in HTB tunnel.

In this paper we present a complete accurate characterization of the average structure of Sb_xWO_{3+y} (x~0.11) by single-crystal X-ray diffraction (XRD) and total energy calculations. The bulk sample has also been investigated by conventional powder XRD methods, scanning electron microscopy (SEM) with energy dispersive spectroscopy (EDS) microanalysis, conventional high-resolution transmission electron microscopy (HRTEM) with EDS analysis and electron diffraction. We have used exit wave reconstruction (EWR) from aberration-corrected TEM images in order to determine the coordination of antimony and oxygen in the hexagonal tunnels and in order to solve the structure of the (3)-ITB phase using statistical parameter estimation theory [11,12]. The positions have been refined in a quantitative way with a precision in the picometer range [13] and been compared with data obtained by single crystal XRD.

Previously EWR has successfully shown local octahedral distortions for the ITB phases [14], where the rotation angle for the octahedra was measured with a precision of ± 0.2° and showed a variation of several degrees. Also a difference in the average rotation angle for WO_6-octahedra in the WO_3-slabs relating to the distance of the interface to the HTB-slab was reported.

Experimental

During a phase analysis study of the antimony tungsten bronze system, an almost single phase sample of a new ternary tungsten bronze, Sb_xWO_{3+y}, was prepared. Sb_2O_3, WO_3 and W-metal powders were ground in an agate mortar in amounts according to the formula $Sb_{0.2}WO_{3.2}$. The powder was then reacted in an evacuated and sealed quartz tube at 950º C for 4 days.

Powder X-ray diffraction (XRD) patterns were recorded with a Guinier-Hägg focusing camera with $CuK\alpha_1$ radiation using Si as an internal standard (a = 5.43085(4) Å [15]). The diffraction profiles were indexed and the unit cell parameters were refined with Pirum, version 921204 [16,17].

The single crystal XRD data collection was done with a Xcalibur-3 equipped with a sapphire-III CCD detector using Mo radiation (λ = 0.71073 Å) on a crystal with a octahedral morphology typical for the larger particles in the batch, shown in Fig 1. The detector was set at 50 mm distance from the crystal. All data processing and corrections of the raw data was done with the CrysAlis software. The structure was solved with direct methods using SHELXS and refined with full matrix least square calculations using SHELXL [18]. All W and Sb atom positions were refined with anisotropic displacement parameters (ADP) with a weak isotropic restraint applied to the ADP's of the Sb atoms. All O atoms were refined with isotropic displacement parameters.

SEM was performed on stub-mounted powder samples using a JEOL JSM 7000F and JEOL JSM 7600F. Selected Area Electron Diffraction SAED and conventional HRTEM studies were performed using a JEOL JEM 2100F (200 kV) and a JEOL JEM 3010 LaB_6 microscope (300 kV). The TEM samples were prepared by crushing a small amount of the bulk sample in an agate mortar and then slurring with n-butanol. The slurry was treated with ultrasound and then drop cast onto a holey carbon film supported on a Cu-grid. EDS analyses were performed on both TEM and SEM instruments using Oxford EDS systems.

For EWR, focal series of 20 images were acquired at 300 kV using a JEOL R005 aberration corrected (S)TEM operated with a spherical aberration of -5µm and using a focal increment of 2 nm. Exit wave restoration was performed using a linear Wiener filter [19] as implemented in the HREM Research software package for Digital Micrograph. Complementary images were acquired using the HAADF imaging mode. Statistical parameter estimation techniques were used to refine quantitative information about the atomic positions from the restored exit wave [11-14].

Total energy calculations within the framework of the density functional theory were carried out using the projector augmented wave method [20] as implemented in the VASP code [21-25]. The Perdew-Burke-Ernzerhof parameterization of the exchange-correlation functional [26,27] and a basis set consisting of plane waves with kinetic energies up to 350 eV were used. Atomic coordinates were taken from the structure refinement on single crystal XRD data. Because disorder, such as the split position of the Sb atoms, can not be treated using the VASP code, all calculations were carried out on ordered model structures. Due to the complexity of the crystal structures, relaxations of atomic coordinates have not been performed. It should be noted that total energies presented here do not correspond to the ground state values, and they are used in this work only to discuss structural trends and experimental observations.

Results

The SEM study showed that the bulk sample contained two different sizes of particles exhibiting different crystal habit, *i.e.* the shape of the crystals, was different (Fig. 1). For the smaller particles the shape is irregular but with facetted faces having an angular relation to each other. The larger particles have a slightly deformed octahedral shape commensurate with the point group symmetry *mm2 (and thus Space group $Pm2_1n$).*

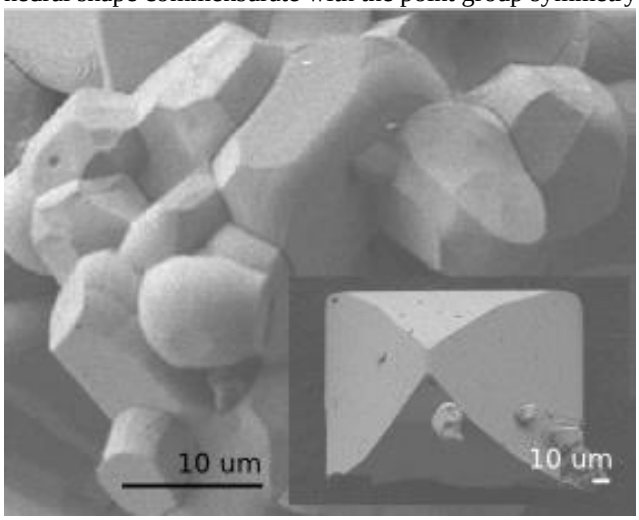

Fig. 1. SEM images, taken with accelerating voltage of 2.0 kV and working distance of 8.0 mm, showing the typical morphology for the agglomerated smaller particles with sizes about 10-20 µm and the ten times larger particle in the inserted image.

The powder X-ray diffraction pattern, shown in Fig. 2, was indexed and refined with the orthorhombic unit-cell: a =27.790(4) Å, b = 7.3671(5) Å and c = 3.8687(5) Å. Only a few weak reflections remained unindexed. The unit-cell dimensions are in good agreement with those previously published for the high-pressure tungsten bronze $La_{0.1}WO_3$ with a (3)-ITB structure [28].

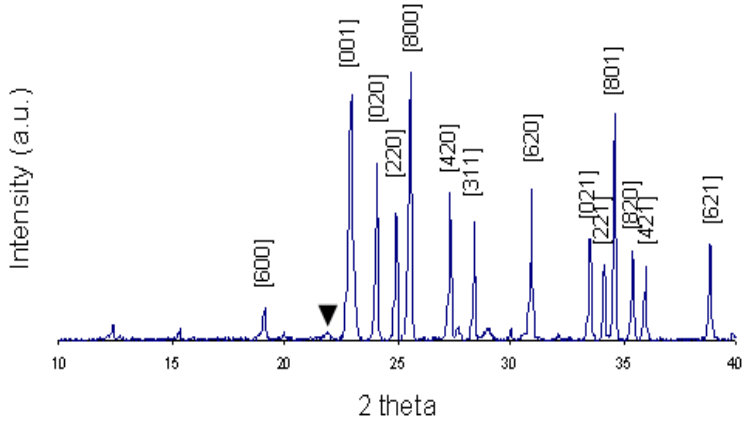

Fig. 2. A part of the powder XRD profile of the bulk sample $Sb_{0.2}WO_{3.2}$. Indices are given for reflections with large intensity and the arrow shows a weak unindexed one.

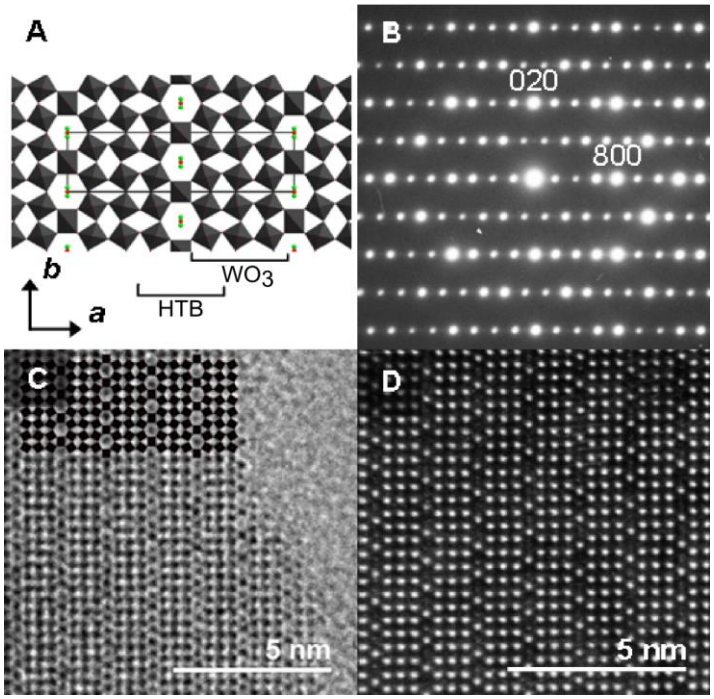

Fig. 3. A: Idealized model of the (3)-ITB structure along [001], with WO_6-octahedra drawn in grey, antimony atoms in green and oxygen atoms as red. The width of the HTB- and WO_3 slabs are marked in the figure. B: The SAED pattern along [001] is characteristic of an ordered (3)-ITB structure. C: HRTEM image with the WO_3 network overlaid in the top part of the image. D: STEM-HAADF image of (3)-ITB along [001] showing the position of the heaviest atomic column containing tungsten with white contrast.

The ITB phases are best identified from SAED patterns and HRTEM images recorded along [001] (Fig. 3). In this orientation it is possible to image the intergrowth arrangement of HTB- and WO_3-slabs since tungsten together with the axial oxygen atoms (…-O-W-O-…), the equatorial oxygen atoms and the tunnel content (…Sb_2O Sb_2O … or …-O-Sb-O-Sb-O-…), respectively, form well-separated columns that lie parallel to the electron beam.

The SAED-pattern (Fig 3B) taken of a thin crystal fragment aligned along the short crystal *c*-axis (3.8 Å) is characteristic of an ordered (3)-ITB phase. The pattern shows the reflection condition $h+k = 2n$. No diffuse streaking or additional reflections can be seen in the pattern. Several (3)-ITB crystals have been investigated by SAED. Diffuse scattering have been observed in a few of the diffraction patterns at $hk0$ $k \neq 2n$. Streaking and additional spots observed along [100] indicate that the (3)-ITB crystal fragment contains defects such as WO_3-slabs of various widths.

In the HRTEM-image taken at Scherzer defocus (Fig. 3C) the black spots correspond to the positions of atomic columns containing heavy atoms as indicated in the overlay. The HTB regions with the single hexagonal tunnel row are separated in the [100] direction by WO_3-slabs (i. e. three layers of octahedra) as is characteristic of the (3)-ITB phase. In the aberration corrected high-angle annular dark field (HAADF) image in Fig. 3D the intensity is approximately proportional to Z^{υ}, where Z is the atomic number and the exponent υ is always smaller than 2 [29]. This image therefore confirms the location of the heaviest atoms (tungsten) in the middle of the octahedra (white dots) and the lighter antimony atoms within the tunnels as very weak white dots.

Several crystals were analyzed by EDS in the SEM microscope (accelerating voltages of 10-20 kV). The microanalyses gave information about the Sb:W ratios in at%. The average antimony content, *x*, was calculated to $x=0.126 \pm 0.008$ giving the formula $Sb_{0.126}WO_{3+y}$. When all hexagonal tunnels in the (3)-ITB structure are fully occupied by Sb-atoms the *x*-value is equal to 0.143 ($x_{max}=0.143$). The EDS-results thus indicate that the hexagonal tunnels are filled to ~90%.

Single-crystal XRD and Total energy calculation

The results from the single-crystal XRD refinement are in good agreement both with the unit cell dimensions of the (3)-ITB phase found by powder XRD and with the results from the electron microscopy study above. It is clear that the structure of the investigated crystal corresponds to that of (3)-ITB. It is likely that the larger crystals contain some local variation in the widths of the HTB- and WO_3-type slabs, however. Such defects are sometimes frequently occurring in ITB materials [29] and will give rise to streaking or additional reflections in the diffraction patterns along the *a*-axis.

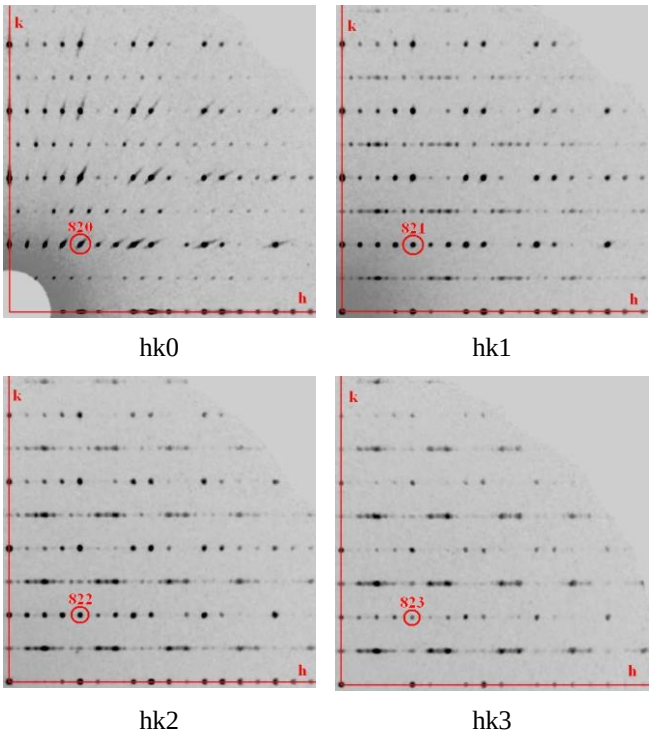

Fig. 4 Reconstructed X-ray diffraction patterns of *hkl* (*l*=0, 1, 2 & 3) planes for (3)-ITB. Only the positive quadrants are shown. The reflections (820), (821), (822) and (823) are shown as encircled reflection spots.

The positive quadrants of orthogonal cuts through the reciprocal space are shown in Fig. 4. In the *hk*0 image very little disorder is visible as density between the diffraction peaks, while in all three other parts of Fig.4, the *hk*1, *hk*2 and *hk*3 projections clearly show signs of considerable disorder as pronounced density in between the diffraction peaks. The *hk*0 projection also clearly shows the reflection condition ($h+k=2n$) due to the *n*-glide perpendicular to the *c*-axis while in the images for the other projections, every k = odd line reveals the weak reflections indicating the 27 Å axis. However when $k = 2n$ the reflections with $h = 2n+1$ (connected with the 27 repetition distance) are either absent or very weak. The dominant character of $k=2n$ reflections could be derived from the fact that the WO_3-part forms a major part of the structure. The structural reasons for the streaking between the $k=2n+1$ reflections indicating some ordering along the *a*-direction (27 Å axis), are not clear for the moment but an hypothesis is that they are connected with disorder among the Sb atoms in the HTB tunnels. The *hk*0 direction would not reveal any disorder of Sb along the *c*-direction but in the other reciprocal planes the disorder is obvious.

Table 1. Crystal data and structural refinement

Crystal data and structural refinement

Empirical formula	$Sb_{0.38}W_{3.50}O_{10.90}$ $(Sb_{0.11}WO_{3.11})$
Formula weight	864.75
Crystal system	orthorhombic
Space group	*Pm2₁n* (no. 31)
Unit cell dimensions	*a* = 27.8135(9) Å
	b = 7.3659(2) Å
	c = 3.8672(1) Å
Cell volume	792.28 $Å^3$
Z	4
Absorpt. Coefficient (mm^{-1})	52.0
F(000)	1461
Crystal size (mm)	0.02 * 0.03 * 0.04
Theta range for data collection (°)	4.02-32.15
Index ranges	$-40 \le h \le 40, -10 \le k \le 10, -5 \le l \le 2$
Reflection collected/unique	14952, 620
Reflections observed [$I > 2\sigma(I)$]	470
Max. and min. transmission	0.12 – 0.35
Data/resistants/parameters	620, 94, 96
Goodness-of-fit on F^2	1.197
Final *R* indices [$I > 2\sigma(I)$]	R_1 = 0.0626
	wR_2 = 0.1726
R indices (all data)	R_1 = 0.0753
	wR_2 = 0.1812
Largest diff. peak and hole ($e/Å^3$)	-5.9 – 6.0
Resolution range (Å)	4.44 - 0.90

Table 2. Atomic coordinates from the single crystal XRD refinement

Atom	Wyck.	Occ.	x	y	z	U
W1	2a	1	0.0000	0.233(2)	0.029(2)	0.0205(16)
W2	4b	1	0.11856(16)	0.5009(5)	0.0485(14	0.0193(13)
W3	4b	1	0.11634(18)	-0.0014(6)	-0.0483(15)	0.0237(14)
W4	4b	1	0.2492(2)	0.5004(13)	-0.0524(10)	0.0227(11)
O1	2a	1	0.0000	0.277(10)	0.496(12)	0.007(19)
O2	4b	1	0.0513(17)	0.066(9)	0.11(2)	0.12(6)
O3	4b	1	0.0491(12)	0.437(7)	0.023(12)	0.000(11)
O4	4b	1	0.1010(18)	0.754(6)	0.006(17)	0.009(11)
O5	4b	1	0.1802(15)	0.518(13)	-0.001(18)	0.05(3)
O6	4b	1	0.1274(17)	0.251(5)	-0.133(12)	0.000(12)
O7	4b	1	0.113(2)	0.500(10)	0.520(10)	0.021(18)
O8	4b	1	0.1825(13)	-0.054(9)	0.003(14)	0.011(15)
O9	4b	1	0.241(2)	0.246(7)	0.00(2)	0.036(19)
O10	4b	1	0.251(3)	0.495(13)	0.468(10)	0.031(17)
O11	4b	1	0.0000	0.81(7)	0.44(12)	0.19(18)
O12	2a	0.80	0.0000	0.797(7)	-0.106(10)	0.017(11)
Sb1	2a	0.27(4)	0.0000	0.662(4)	0.004(9)	0.025(8)
Sb2	2a	0.5	0.0000	0.233(2)	0.029(2)	0.0205(16)

I

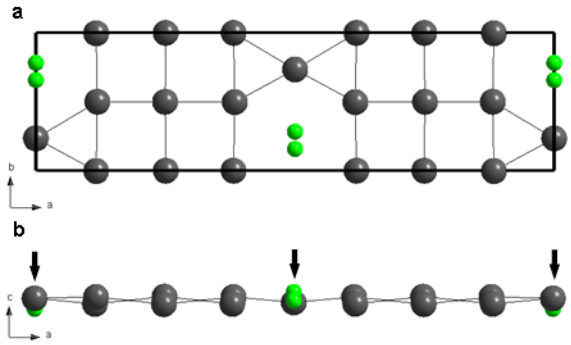

Fig. 5. Structural models obtained from the single crystal XRD refinement projected along the [001] (a) and [010] (b). W-atoms are connected and shown in grey and Sb-atoms in green. In b) three W-atoms in the HTB-slab (indicated with an arrow) are on nodal positions and the W-atoms between them (WO_3-type slab) are oscillating in the *c*-direction. Oxygen atoms (not shown) are located near the lines connecting W atoms in the *ab* plane and between W atoms along c and also in the hexagonal channels.

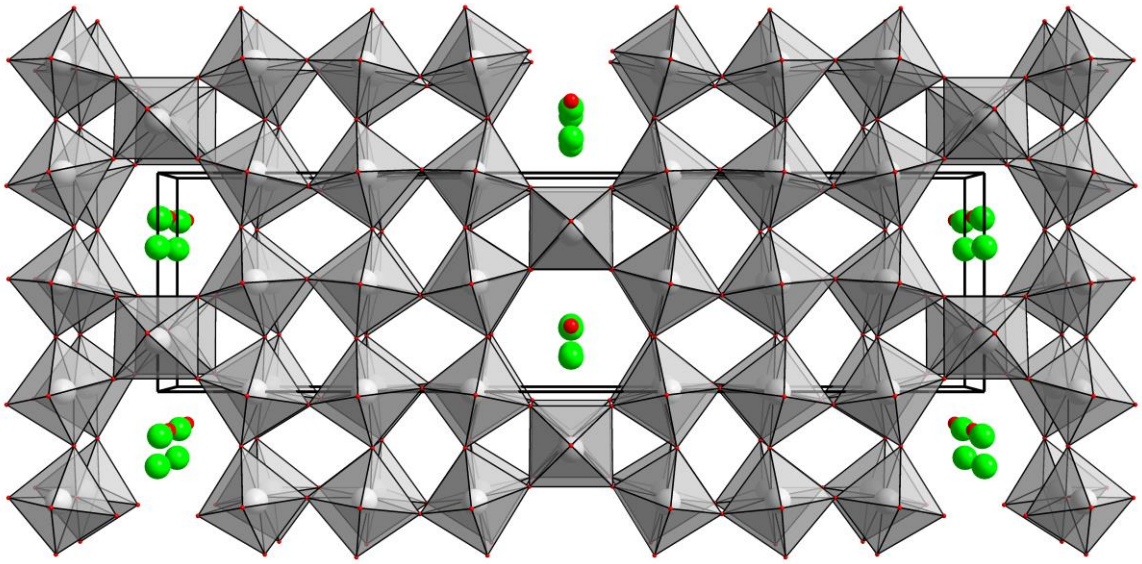

Fig 5c. Perspective view along the *c*-axis of a polyhedral model of the 3-ITB structure

The positions for W are highly regular in the *ab*-plane as can be seen in Fig. 5a, but the height along the c-axis is fluctuating in a wavelike manner (Fig. 5b). This wavelike fluctuation is influenced also by the Sb-atom position. In this case the Sb position, which is filled to 80 %, should have the largest influence. The WO_6-octahedra contains distortions in the oxygen atom arrangement and especially for the octahedra closest to the hexagonal tunnel and the antimony atoms.

From the single-crystal XRD results the content of the hexagonal tunnels consists of a pair of partially occupied antimony atoms and oxygen ions in a chain. The single-crystal XRD gives a split in the position for Sb in the hexagonal tunnel with a shortest interatomic distance of 1.036(38) Å. For the split position on Sb one of the positions (labeled Sb1 in Table 2) is filled to 27% whereas the other one (Sb2) to 50% agreeing to the fact that the positions can not be filled at the same time, due to steric reasons. The structure of the (2)-ITB in the Sb-W-O system has previously been determined from single-crystal X-ray diffraction and electron diffraction, where the Sb^{3+} ion in the hexagonal tunnel was also reported to be displaced from the central position. The two positions have slightly different surroundings and locations in the hexagonal tunnel. For the Sb-atom position occupied to 50% (Sb2) the distances to the closest O-atoms are close to the value calculated by the bond valence method for the bond, r_o, between Sb^{3+} and O^{2-} in Sb_2O_3 determined to be 1.927 Å by bond-valence model [30]. The location of the Sb-position occupied to 27% (Sb1) is slightly above the W-atoms in the [001]-direction of the unit cell. The bond lengths for this position are not as ideal and thus the distances of the bonds indicates that the location for the Sb-position filled to 50% is more favourable. The presence of a non-ideal environment around the Sb1 position (27 % occupancy) is corroborated by total energy calculations: An ordered model where only the Sb2

position is occupied is 3.35 eV per Sb atom more stable than a model where only the Sb1 position is occupied. This is a very large energy difference considering that only the position of a single atom is changed, and it suggests that oxygen atoms near the Sb1 sites may also shift. This could be a reason for the large thermal displacement parameter of oxygen atoms inside the hexagonal channels (labelled O12 in Table 2).

The Sb atoms could be arranged in Sb-O-Sb dimers, as reported by Parmentier et al. for a (2)-ITB phase in the Sb-Mo-O system [10] or in -Sb-O-Sb-O-Sb- chains, as shown in Fig. 6. This means that each antimony atom has a surrounding of SbO_3E-type or SbO_4E-type, with E being a lone pair. Both situations were compared by total energy calculations, considering the reaction

$2\ Sb_2W_{14}O_{44} \rightarrow Sb_4W_{28}O_{86} + O_2$

Here, $Sb_4W_{28}O_{86}$ denotes an ordered superstructure with doubled c axis, where every other O atom in the channel is removed. Both possibilities of placing the Sb atoms were taken into account, and they lead to qualitatively same results: both reactions are endothermic (147 kJ/mol or 189 kJ/mol when Sb is placed on Sb1 or Sb2, respectively), but the entropy contribution will shift the equilibrium to the right side at approximately 720 K or 920 K (estimated using $\Delta H - T\Delta S°(O_2) = 0$). The actual oxygen content in the tunnel may therefore depend strongly on the reaction conditions and especially the reactivity of the material during cooling.

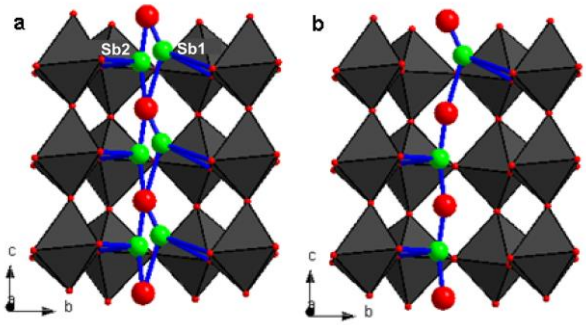

Fig. 6. Cross-section of the hexagonal tunnels in a structural model of the single crystal XRD refinement results with a) showing both the Sb-atoms (green) drawn in and b) with only one of the positions occupied.

Table 3. Selected interatomic distances.

	Sb1 (27% occ.)	Sb2 (50% occ.)
O_{octa}*	2.57(9) Å	2.15(5) Å

*Oxygen in the WO_6-octahedra, **oxygen in the hexagonal tunnel.

From the structural refinement the structure composition is calculated to $Sb_{0.11}WO_{3.11}$ which corresponds to 80% filling of the hexagonal tunnels. This value is slightly lower than the average x-value = 0.126 (90% filling) obtained from the electron microscopy study (see above). The results clearly show that the hexagonal tunnels are not completely filled and that the Sb-content in the tunnels slightly vary from crystal to crystal. This is in agreement with previous results reported for intergrowth tungsten bronzes [28,31]. The chemical formula $Sb_{0.11}WO_{3,11}$ (80% filling) gives an average oxidation state of 5.89 for tungsten. The color, dark blue, also suggests that tungsten is slightly reduced in the title compound. This is confirmed by inspecting the electronic density of states, DOS (Fig. 7), calculated for full occupation of the Sb2 site inside the tunnels), which consists of four groups of peaks. The lowest group, about 20 eV below the Fermi energy, is made up mostly of oxygen s states. The second and third groups between -12 eV and -2 eV contain the Sb-O and W-O bonding states. These are oxygen majority states, corresponding to polar covalent bonds due to the larger electronegativity of oxygen compared to Sb or W. The Fermi level cuts the fourth group, the conduction band, which is mainly composed of tungsten d states. This reflects the slight reduction of tungsten, which is responsible for the dark color of the title compound.

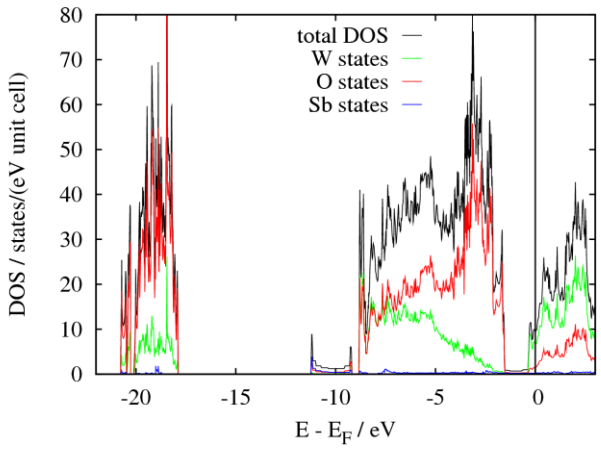

Fig. 7. DOS. Electronic density of states of the (3)-ITB. Only the Sb2 position is fully occupied with Sb.

Exit wave reconstruction

Exit wave reconstructions from defocus series was measured for several crystals along [001]-direction. The result gives information about the phase and amplitude of the exit wave. In Fig.4, where the phase of the reconstructed exit wave is imaged, the white spots correspond to the positions of atomic columns. This reconstructed phase reveals the majority of the pure oxygen columns unlike the single HRTEM-image where only the heavier atomic columns are observable [14]. Simulations show that unfortunately even at a resolution better than 0.9 nm it is not possible to resolve the oxygen column from the antimony atoms inside the tunnel sites.

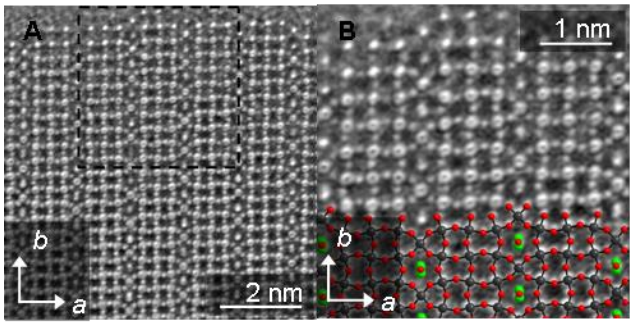

Fig. 8. Phase images of the exit wave restoration with the area marked in A) enlarged in B) with the atomic structure overlaid.

It is clear that the intensities of atomic columns in the main framework are relatively uniform across the full region shown in the restoration. In contrast, the intensities of the atomic columns within the hexagonal show more pronounced variations in both position and magnitude. However, the average position of the atomic site for the antimony is not in the centre of the hexagonal tunnel as can be seen in the structural model shown in Fig 1 A. This may be a charge balancing effect whereby the +III charge on the antimony ions needs to be balanced and thus the ions form bonds with the neighbouring oxygen atoms in the framework. This displacement of the tunnel content in the ab-plane seems to be predominantly in the b-axis direction, towards the octahedra in between the hexagonal tunnels. This implies that the antimony position depends on the wider bonding environment and not only on the nearest neighbour octahedra since in this case displacements towards the other octahedra in the WO_3-slab would be expected to be equally beneficial. The reason for this preferred direction of the displacement is probably related to the symmetry of the position, where the displacement in toward the HTB-WO_6 will not break the symmetry.

Statistical parameter estimation

A small region of the phase of the exit wave, shown in figure 8A, has been analyzed in a quantitative way using statistical parameter estimation theory. This requires a model-based approach where the phase of the exit wave is considered as a data plane from which the unknown parameters can be estimated in a statistical way. The

phase of the reconstructed exit wave is modeled as a superposition of Gaussian peaks. The expectations at the pixel *(k,l)* at the position (x_k,y_l) are given by[14]:

$$f_{kl}(\theta) = \zeta + \sum_{i=1}^{I}\sum_{m_i=1}^{M_i} \alpha_{m_i} \exp\left(-\frac{(x_k - \beta_{x_{m_i}})^2 + (y_l - \beta_{y_{m_i}})^2}{2\rho_i^2}\right) \qquad (1)$$

where ζ is a constant background, α_{m_i} and ρ_i are the column type dependent height and width of the Gaussian peak, respectively, $\beta_{x_{m_i}}$ and $\beta_{y_{m_i}}$ are the *x* and *y* coordinate of the m_ith atom column, respectively. In this expression, the index *i* refers to a particular column type and the index m_i refers to the *m*th column of column type *i*. The unknown parameters $\theta = \left(\beta_{x_{1_1}},\ldots,\beta_{x_{M_I}},\beta_{y_{1_1}},\ldots,\beta_{y_{M_I}},\rho_1,\ldots,\rho_I,\alpha_{1_1},\ldots,\alpha_{M_I},\zeta\right)^T$ of the model are estimated in the least squares sense. The uniformly weighted least squares estimates $\hat{\theta}$ are given by the values of *t* that minimize the uniformly weighted least squares criterion[12,13]:

$$\hat{\theta} = \arg\min_t \sum_{k=1}^{K}\sum_{l=1}^{L}(w_{kl} - f_{kl}(t))^2 \qquad (2)$$

where w_{kl} is the value of the reconstructed phase at the pixel *(k,l)*.

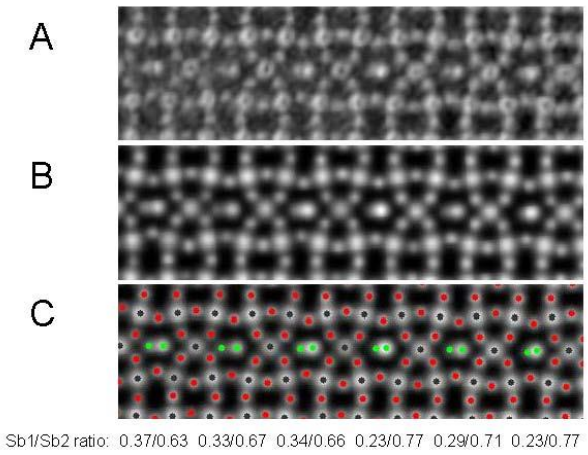

Fig. 9. Statistical parameter estimation results obtained from a local area A: part of the experimental phase image; B: model for the phase evaluated at the estimated parameters; C: an overlay indicating the estimated positions of the different types of atom columns (green Sb, red O and gray W). The estimated intensity ratio is indicated for each Sb-Sb atomic column pair.

The refined model, that is Eq. (1) evaluated at the estimated parameters, is shown in figure 9B and 9C, showing a good visual correspondence between the experimental phase and the model. However, as mentioned previously the resolution was insufficient to resolve the oxygen atoms in between the antimony atoms in the tunnel positions. From the estimated Sb atomic positions, the mean separation between the two displaced Sb atomic columns from the centre was calculated to be 1.10 ± 0.05 Å. Furthermore, for each pair of Sb columns in a hexagonal tunnel, the peak intensities have been quantified. From this analysis, it is observed that the intensity is not equally distributed between the sites. The actual ratios are indicated at the bottom of figure 9C. For the local area analyzed in Fig. 9, the mean intensity ratio equals 0.43 ± 0.05 being in excellent agreement with the 0.54/1.00 ratio found from the refinement of occupational parameters in the single crystal XRD analysis (see Table 2).

Structural communication between adjacent hexagonal tunnels

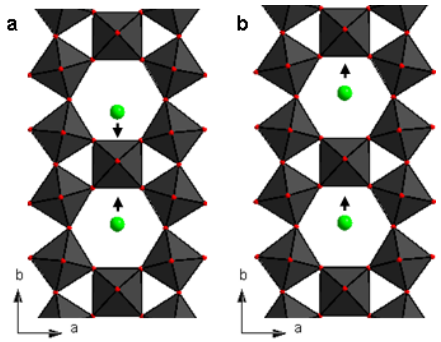

Fig. 10. Hypothetical models of the position for Sb in two adjacent hexagonal tunnels. Shown for the (3)-ITB structure in the [001]-direction, with WO_6-octahedra drawn in grey and Sb-atoms in green.

This strengthens the implication that there is a structural communication between the tunnel sites for antimony, where the filling of one tunnel site is dependent on the filling of adjacent tunnels and thus a trend will be continued from one hexagonal tunnel to the next. The trend that is observed most commonly experimentally between adjacent hexagonal tunnels in the *b*-axis direction is shown in Fig. 10b. In order to rationalize this trend, total energy calculations have been performed on three model structures, all of which contain –Sb-O- chains in the channels: in addition to the two models described earlier, (a) Sb only on the Sb1 site and (b) Sb only at the Sb2 site, a twofold superstructure with doubled b axis (model c), which corresponds to half-occupied Sb1 and Sb2 sites, is considered. Both, models (a) and (b) correspond to the arrangement shown in Fig. 10b, whereas model (c) corresponds to the arrangement shown in Fig. 10a. It turns out that the total energy of model (c) is 0.59 eV higher than the sum of total energies of (a) and (b). Therefore, the arrangement shown in Fig. 10b is expected to be more favorable, in agreement with experimental observation.
The bonding to the neighboring oxygen atoms in the main framework might also lead to a small displacement of the tungsten in between the hexagonal tunnels. Both the dimers and the chains will correlate through the layers in the direction of the *c*-axis and thus communication of the structural positions can be spread in the *c*-direction. This means that the positions of the antimony, e.g. the direction of the displacements, could also be correlated throughout the short *c*-axis although the geometry of the structure mean that this is difficult to observe using HRTEM.

Concluding remarks

The paper clearly shows that the combination of exit wave reconstruction with statistical parameter estimation theory can obtain valuable information about fluctuations and local ordering which cannot be obtained through single-crystal XRD.
The average crystal structure of a new antimony tungsten bronze, Sb_xWO_{3+y}, was determined by single crystal X-ray diffraction. It belongs to the class of intergrowth tungsten bronzes, where hexagonal channels formed by WO_6 octahedra are separated in one direction by WO_3-type slabs three WO_6 -octahedra wide. The hexagonal channels are filled with Sb and O atoms. Sb atoms are displaced from the channel center, resulting in a split atom position. By exit wave reconstruction from through-focus series of HRTEM images in combination with statistical parameter estimation, it is possible to quantitatively study local fluctuations in the Sb site occupancy and positions in a quantitative manner, which is impossible by X-ray diffraction or total energy calculations. Sb atoms in adjacent channels tend to be displaced in the same direction, but the ratio of the occupation of the two possible Sb positions varies from channel to channel. Total energy calculations do support the experimental findings, but the complexity of the crystal structure, and in particular the local ordering, impedes a quantitative treatment.

Acknowledgements. This work was supported by the Swedish Research Council (VR), Berzellii Centre EXSELENT and Knut and Alice Wallenbergs foundation in Sweden, and WCU program (R-31-2008-000-10055-0), Korea. A. De Backer and S. Van Aert gratefully acknowledge financial support from the Fund for Scientific Research Flanders (FWO) through project fundings (G.0188.08 and G.0064.10N) and a Ph.D. research grant to A. De Backer. Financial support from the European Union for the Framework 6 programme under a contract for an Integrated Infrastructure Initiative (reference 026019 ESTEEM) is acknowledged. SJ Haigh and A.I. Kirkland gratefully acknowledge financial support from EPSRC (grant EP/F048009/1) and JEOL (UK) Ltd.

References

[1] T. Ekström, R. J. D. Tilley: The Crystal Chemistry of the Ternary Tungsten Oxides. Chemica Scripta, **1980**, 15, 1-23.

[2] B. Broyde: Tungsten Bronze Fuel Cell Catalysts. J. Catalysis, **1968**, 10, 13-18.

[3] H.R. Shanks, A.J. Bevolo, G.C. Danielson, M.F. Weber: Fuel cell oxygen electrode. US patent, US4232097, **1980**.

[4] B. Xue, J. Peng, Z.F. Xin, Y.M. Kong, L. Li, B. Li: High-contrast electrochromic multilayer films of molybdenum-doped hexagonal tungsten bronze ($Mo_{0.05}$-HTB) . J. Mater. Chem., **2005**, 15, 4793-4798.

[5] I. Tsuyumoto, T. Kudo: Humidity sensor using potassium hexagonal tungsten bronze synthesized from peroxo-polytungstic acid. Sensors and Actuators B: Chemical, **1996**, 30, 95-99.

[6] Y.S. Lim, S.H. Jung, S.-T. Hong, S.M. Jung, J. Kim, J.H. Chae, W.-H. Lee: A structural analysis of W-Sb mixed oxide catalyst. Appl. Surf. Sci, **2005**, 252, 976-980.

[7] A. Magnéli: Studies on the Hexagonal Tungsten Bronzes of Potassium, Rubidium and Cesium. Acta Chem. Scand. **1953**, 7, 315-324.

[8] A. Hussain, L. Kihlborg: Intergrowth Tungsten Bronzes. Acta Crystallogr. A, **1976**, 32, 551-556.

[9] S.T. Triantafyllou, P.C. Christidis, C.B. Lioutas: An X-Ray and Electron Diffraction Study of the Intergrowth Tungsten Bronze $Sb_{0.16}WO_3$. J. Solid State Chem., **1997**, 134, 344-348.

[10] M. Parmentier, C. Gleitzer, A. Courtois, J. Protas: Structure Cristalline de $Sb_2Mo_{10}O_{31}$. Acta Crystallogr. B, **1979**, 35, 1963-1967.

[11] den Dekker, A. J.; Van Aert, S.; van den Bos, A.; Van Dyck, D.; Chen, J. H.: Maximum likelihood estimation of structure parameters from high resolution electron microscopy images. Part I: A theoretical framework. Ultramicroscopy, 2005, 104, 83-106.

[12] S. Van Aert, A.J. den Dekker, A. van den Bos, D. Van Dyck J.H. Chen: Maximum likelihood estimation of structure parameters from high resolution electron microscopy images. Part II: A practical example. Ultramicroscopy, **2005**, 104, 107-125.

[13] S. Bals, S. Van Aert, G. Van Tendeloo, D. Ávila-Brande: Statistical Estimation of Atomic Positions from Exit Wave Reconstruction with a Precision in the Picometer Range. Phys. Rev. Lett., **2006**, 96, 096106.

[14] A.I. Kirkland, J. Sloan, S. Haigh: Ultrahigh resolution imaging of local structural distortions in intergrowth tungsten bronzes. Ultramicroscopy, **2007**, 107, 501-506.

[15] D. Yoder-Short: On a small error in SRM640, SRM640a and SRM640b lattice parameters. *J. Appl. Cryst.* (**1993**) 26, 272-276

[16] L. Eriksson, P.-E. Werner: Computer program PIRUM, version 921204, Stockholm University, (**1992**).

[17] P.-E. Werner: A Fortran program for least-squares refinement of crystal-structure cell dimensions..*Arkiv Kemi*, (**1969**), 31**,** 513–516.

[18] G.M. Sheldrick: A short history of SHELX, Acta Crystallogr. (**2008**), A64, 112-122

[19] A.I. Kirkland, R.R. Meyer: Indirect transmission electron microscopy; Aberration measurement and compensation and exit wave reconstruction. Inst. Phys. Conf. Ser. **2004**, 331-336.

[20] P.E. Blöchl: Projector augmented-wave method. Phys. Rev., **1994**, B 50, 17953.

[21] G. Kresse, J. Hafner: Ab initio molecular dynamics for liquid metals. Phys. Rev., 1993, B 47, 558.

[22] G. Kresse, J. Hafne.: Ab initio molecular-dynamics simulation of the liquid-metal-amorphous-semiconductor transition in germanium. Phys. Rev., **1994**, B 49, 14251.

[23] G. Kresse, J. Furthmüller: Efficiency of ab-initio total energy calculations for metals and semiconductors using a plane-wave basis set. Comput. Mat. Sci., **1996**, 6, 15.

[24] G. Kresse, J. Furthmüller: Efficient iterative schemes for ab initio total-energy calculations using a plane-wave basis set. Phys. Rev., **1996**, B 54, 11169.

[25] G. Kresse, D. Joubert: From ultrasoft pseudopotentials to the projector augmented-wave method. Phys. Rev., **1999**, B 59, 1758.

[26] J.P. Perdew, K. Burke, M. Ernzerhof: Generalized gradient approximation made simple. Phys. Rev. Lett., **1996**, 77, 3865-3868.

[27] J.P. Perdew, K. Burke, M. Ernzerhof, M.: Erratum: Generalized gradient approximation made simple. Phys. Rev. Lett., **1997**, 78, 1396.

[28] C. Grenthe, M. Sundberg, V.P. Filonenko, I.P. Zibrov: High-pressure tungsten bronzes, RE_xWO_3 with *RE*=La and Nd, studied by X-ray diffraction and Electron Microscopy. J. Solid State Chem. **2000**. 154, 466-475.

[29] P. Hartel, H-Rose. C.Dinges; Conditions and reasons for incoherent imaging in STEM. Ultramicroscopy 1996, 63, 93-114.

[30] V. Sidey: On the accurate bond-valence parameters for the Sb^{3+}/O^{2-} ion pair. Acta Crystallogr., 2010, 66, 307-314.

[31] L. Kihlborg, H. Blomqvist, M. Sundberg: Low Members of the Intergrowth Tungsten Bronze Family by Partial Substitution of Molybdenum for Tungsten. J. Solid State Chem., **2001**, 162, 341-346.